Journal of Materials Chemistry A

Tetrathiafulvalene (TTF) Derivatives as Catholytes for Dual-Type Redox Flow Batteries: Molecular Engineering Enables High Energy Density and Cyclability

Journal:	*Journal of Materials Chemistry A*
Manuscript ID	TA-ART-06-2023-003606.R1
Article Type:	Paper
Date Submitted by the Author:	16-Aug-2023
Complete List of Authors:	Wang, Xiao; University of Cincinnati, Chemistry Lashgari, Amir; University of Cincinnati, Chemistry Siwakoti, Rabin; University of Cincinnati, Chemistry Gautam, Rajeev; University of Cincinnati, Chemistry McGrath, Jack; University of Cincinnati, Chemistry Sarkar, Prasenjit; University of Cincinnati, Chemistry Naber, Grace; University of Cincinnati, Chemistry Chai, Jingchao; University of Cincinnati, Chemistry Jiang, Jianbing; University of Cincinnati, Chemistry

ARTICLE

Tetrathiafulvalene (TTF) Derivatives as Catholytes for Dual-Type Redox Flow Batteries: Molecular Engineering Enables High Energy Density and Cyclability

Received 00th January 20xx,
Accepted 00th January 20xx

DOI: 10.1039/x0xx00000x

Xiao Wang,[a,‡] Amir Lashgari,[a,‡] Rabin Siwakoti,[a] Rajeev K Gautam,[a] Jack J. McGrath,[a] Prasenjit Sarkar,[a] Grace Naber,[a] Jingchao Chai,[a] Jianbing "Jimmy" Jiang[a,*]

Redox flow batteries (RFBs) have received increasing attention on large-scale energy storage owing to their ability to decouple energy and power. Despite remarkable progress, the application of RFBs is greatly restricted by their limited energy density, resulting from the limited solubility of the redox species. It is still challenging to develop RFBs with high energy density and cyclability owing to the inherent instability of redox materials and high-concentration-induced parasitic reactions. Herein, we demonstrate the viability of a new family of redox compounds, tetrathiafulvalenes (**TTF**s), in both slurry- and solution-based RFBs using aqueous and nonaqueous electrolytes, respectively. In former batteries, pristine **TTF** was derivatized with four cyanoethyl chains (**CN-TTF**) to suppress the solubility and obtain suspended **CN-TTF** in an aqueous electrolyte as a slurry. The incorporation of the hydrophobic chains into **TTF** enhanced the redox stability by suppressing the dimerization of **TTF** while preserving the highly stable redox properties of **TTF**, resulting in a capacity retention of 75.8% after 1000 cycles (99.97% per cycle) (226 h, 9.4 d). Furthermore, **TTF** was derivatized with four poly(ethylene glycol) chains (**PEGn-TTF**, n = 1 and 3) to obtain a concentration of 0.5 M in a carbonate electrolyte, corresponding to an electron concentration of 1.0 M. When paired with Li as the anode, the solution-based battery exhibited a cell voltage of 3.64 V and a capacity retention of 82.9% after 18.5 d and a high energy density of 88 Wh/L. This study introduces a new family of organic compounds for the dual-type flow battery applications and provides molecular design principles for the development of robust organic materials with desirable properties for large-scale energy storage.

Introduction

Large-scale energy-storage devices are required to mitigate the intermittency of renewable energy sources.[1,2] Solid-state batteries, an important part of energy-storage systems, are now widely applied in various fields because of their advantages in terms of energy density and operating time. Li-ion batteries, known as one of the most successful solid-state batteries, have become indispensable components of portable electronics and electric vehicles.[3,4] Redox flow batteries (RFBs) utilize liquid electrolytes with redox species in external tanks and thus possess the capability to decouple the energy and power densities.[5-11] However, owing to the low cell-operation voltage and limited concentration of the active material, the energy density of RFBs (25 Wh/L) is much lower than that of commercial Li-ion batteries (800 Wh/L).[12-14] The energy density of RFBs is dependent on the solubility of the electroactive materials, number of electrons transferred, and cell voltage.[15]

With the development of RFBs based on organic materials, wherein organic molecules serve as redox compounds, a significant number of organic compounds can be utilized as redox materials. Organic compounds, such as anthraquinone, ferrocene, benzoquinone, viologen, phenothiazine, and 2,2,6,6-tetramethylpiperidine-1-oxyl (TEMPO), have been extensively investigated in organic RFBs.[16-27] Molecular engineering can increase the solubility of organic redox compounds in electrolytes and tune the redox potential of organic compounds.[22,28] For example, the attachment of polar substituents, such as sulfonate and ethylene oxide, has been shown to alter the solubility of anthraquinone.[29-31] The replacement of the strongly polar chloride anions of methyl viologen with nonpolar bis(trifluoromethanesulfonyl)imide ions increased the solubility of the product in nonaqueous electrolytes in relation to that of the parent molecule.[32] The potential tuning of common redoxmers, such as ferrocene and methyl viologen, can be realized by introducing electron-withdrawing/donating groups adjacent to the redox center.[33,34] Despite remarkable progress, the development of redoxmers with high voltage, high energy density, and long-term battery cyclability is still challenging. The versatile features of RFBs allow the use of redox materials in both slurry and solution states to utilize the advantage of the solubility properties of different redoxmers. Redox materials with high solubility are suitable for solution-based RFBs, while materials with low solubility can be applied to slurry batteries.

While solution-based RFBs are superior to the previously reported RFBs, slurry batteries have gained increasing attention owing to their high energy densities. The direct utilization of

[a] *Department of Chemistry, University of Cincinnati, P.O. Box 210172, Cincinnati, Ohio 45221-0172, United States*
**Corresponding author: jianbing.jiang@uc.edu.*
‡ Equal contribution
Electronic supplementary information (ESI) available. See DOI:

insoluble materials in RFBs is one means of exploiting the higher energy density of traditional solid-state batteries and the scalability of solution-based RFBs.[35,36] Wang *et al.* proposed redox-targeting flow batteries using soluble redox materials as mediators. The essence of this strategy is to relay electrons between the electrode, redox mediator, and solid-state redox material.[37-40] Although this strategy has advanced the development of RFBs with high energy density, the intrinsic voltage loss and difficulty in matching the redox potentials between the mediator and the active material also limit the utility of this approach. By contrast, to avoid the use of a redox mediator, a flowable redox suspension is directly employed as the electrolyte for the battery, thereby broadening the scope of redox compounds as electrolytes. Slurry batteries based on both organic and inorganic species, including multi-electron active polyhydroquinone, carbon-coated 10-methylphenothiazine, and carbon-coated binder-based $CuSi_2P_3$, have been demonstrated.[36,41-44]

Tetrathiafulvalene (**TTF**) derivatives were originally synthesized by Wudl *et al.* in the 1970s as strong electron-donating molecules for use as organic conductors.[45,46] As non-aromatic conjugated organic compounds, **TTFs** possess excellent redox properties, undergoing two successive one-electron redox processes at 0.34 V vs. Ag/AgCl (**TTF**/**TTF**$^{+\bullet}$) and 0.78 V vs. Ag/AgCl (**TTF**$^{+\bullet}$/**TTF**$^{2+}$**)** in MeCN.[47] In many studies, **TTF** has been proven to be thermodynamically and electrochemically stable in various environments.[47-49] Owing to this characteristic feature, **TTF** and its derivatives have been used as organic electrodes in energy-storage systems.[50-52]

Herein, we derivatized **TTF** with different functional groups (**CN-TTF** and **PEG3-TTF**) to confer distinct physical and electrochemical properties to the slurry- and solution-based RFBs in the aqueous and nonaqueous electrolytes, respectively (Figure 1A). The functionalization of **TTF** with cyano-terminated alkyl chains (**CN-TTF**) is expected to not only suppress the dimerization of the **TTF** moieties but also increase the redox potential due to the electron-withdrawing nature of the cyano units. Cyclic voltammetry (CV), battery cycling studies revealed that incorporating sulfur-containing alkyl chains with cyano units as terminal groups into **TTF** inhibits the dimerization of the aromatic core of **TTF** during the redox reaction, which consequently enhances the cyclability of the battery. Compared to the performance of the 0.5 M **TTF** battery (the capacity retention of 46.9% after 50 cycles, average Coulombic efficiency of 96.2%), the battery with 0.5 M **CN-TTF** shows a capacity retention of 82.2% and an average Coulombic efficiency of 97.6% after 400 cycles. **CN-TTF** showed improved kinetic properties in relation to **TTF** and exhibited excellent cycling performance, and the battery employing 1.0 M **CN-TTF** afforded 75.8% capacity retention after 1000 cycles. Paired with Li metal, the two-electron-active poly(ethylene glycol)-derivatized **TTF** (**PEG3-TTF)** exhibits high battery voltages of 3.44 and 3.64 V and an excellent capacity retention of ~83% after 100 cycles (after 18 d) (99.87% per cycle) at a high electron concentration of 1.0 M. The high solubility, multi-electron activity, and high voltage of **PEG3-TTF** result in an energy density of 88 Wh/L.

Results and discussion

Molecular design and synthesis. Numerous molecular engineering strategies, including tuning the redox potential and enhancing the solubility, have been reported to optimize the redoxmer properties.[53] Here, different functional groups were incorporated into the TTF core to achieve different physical and electrochemical properties: (1) four cyanoethyl chains were attached to the TTF framework to not only suppress the dimerization of pristine TTF[54] but also anodically shift the redox potential to a higher cell voltage for slurry RFBs in an aqueous electrolyte (Figure 1A); and (2) four PEG chains were incorporated to achieve a higher solubility in an organic electrolyte and increase the molecular size for mitigated crossover (Figure 1A). The three analogous compounds, CN-TTF, PEG1-TTF (with one ethylene glycol unit), and PEG3-TTF (with three ethylene glycol units), were purified and characterized prior to electrochemical and battery-cycling measurements (see Supplementary Information).

Solubility. Owing to the high hydrophobicity of the **TTF** framework, all **TTF** compounds have low solubility in water (less than 1 mM, Table S1 and Figure S1A), which is consistent with a previous report.[55] However, even though the incorporation of the cyano units did not improve the solubility of **CN-TTF** in water, its dispersity in water significantly improved, presumably because of the tendency of the cyano groups to form hydrogen bonds (Figure S1). This phenomenon allows the preparation of a slurry with uniformly suspended **CN-TTF** for subsequent battery studies. In terms of

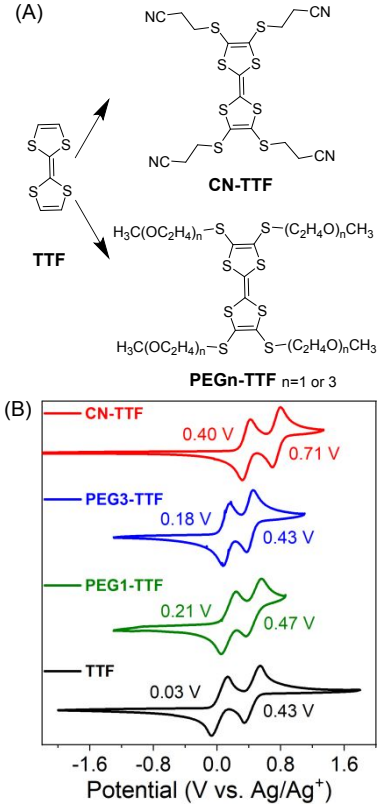

Figure 1. (A) Chemical structures of **TTF**, **CN-TTF**, and **PEGn-TTF**. (B) Cyclic voltammograms of 1 mM **TTFs** in 0.1 M tetrabutylammonium hexafluorophosphate ($TBAPF_6$)/acetonitrile (MeCN) at a scan rate of 50 mV/s.

solubility in organic solvents, **TTF** presents a solubility of 0.1 M in MeCN and 0.23 M in propylene carbonate (PC). The attachment of the four cyano units decreased the **CN-TTF** solubility in both the PC and MeCN systems (less than 25 mM). By contrast, the introduction of the PEG groups had a significant impact on solubility: the solubility of the **PEG1-TTF** powder attained 270 mM and 350 mM in MeCN and PC, respectively. **PEG3-TTF** with longer PEG chains is an orange liquid that is miscible with MeCN and PC. **PEG3-TTF** possesses the highest solubility in organic solvents, and thus it is the primary focus of solution-based flow battery studies.

Electrochemical properties. The electrochemical properties of the soluble **TTFs** were characterized by CV plots recorded in different systems. **TTF** undergoes two single-electron reactions at 0.1 V and 0.43 V vs. Ag/Ag^+ (Figures 1B and S2A). During the first redox reaction, TTF releases one electron, yielding a carbon radical ($TTF^{\bullet+}$), which can be further oxidized to afford TTF^{2+}. As expected, the –CN modified compound, **CN-TFF**, also presented two redox couples at higher potentials of 0.40 V and 0.71 V vs. Ag/Ag^+ due to the electron-withdrawing effect of the ethyl cyanide chains. In addition, the electron-withdrawing effect of a sulfur linkage in **PEG1-TTF** and **PEG3-TTF** slightly increases the potential by 0.03–0.1 V (Figure 1B). During oxidation, the **TTF** core releases one electron to form a cationic radical ($\mathbf{TTF^{+\cdot}}$), which subsequently undergoes a second electron oxidation to produce $\mathbf{TTF^{2+}}$ with two positive charges.[47,56]

The redox properties of redoxmers are significantly affected by the electrolyte system (salts and solvents).[57-59] To optimize the electrochemical behavior of **PEG3-TTF**, different electrolyte systems (Figure S2) were used, including Li salt/carbonate, quaternary ammonium/MeCN, and sodium perchlorate/MeCN and PC systems. **PEG3-TTF** presents consistent electrochemical potentials in the different electrolyte systems with the first electron at 0.19–0.24 V vs. Ag/Ag^+ and the second at 0.37–0.44 V vs. Ag/Ag^+. This study indicates that the electrochemical performance of **PEG3-TTF** is invariable to the electrolyte system and that **PEG3-TTF** is a robust material for battery applications.

Cyclic voltammograms were also studied to understand the redox stability of the different **TTF** molecules. **CN-TTF** was first subjected to low-scan-rate (5 mV/s) CV measurements (Figure S3); it exhibited high redox reversibility, as evidenced by the ratio of the cathodic to anodic current (i_{pc}/i_{pa} = 1.01 for the first reduction couple and 1.05 for the second) and the Nernstian-peak separations for one-electron redox processes (73 mV for the first reduction and 82 mV for the second reduction, Table S2). Long-term CV-cycling tests were conducted to further evaluate the electrochemical stability (Figure S4). No distinct difference in the current density and potential was observed for **CN-TTF** at the 1st and 100th cycles, suggesting no distinct detrimental effect of side chains on the redox stability of the **TTF** unit.[49] In all systems (Figure S5–S11), **PEG3-TTF** exhibited two consecutive one-electron redox processes, as evidenced by the two redox peaks, a peak separation (~59 mV), and a high redox reversibility (peak current ratio ~1) (Table S3). After 100 cycles, no distinct changes in the redox potential or peak current intensity were observed (Figures S5–S11)., suggesting that the **PEG3-TTF** electrolyte could be suitable candidates for the subsequent battery performance studies.

Electrokinetics. The electrochemical kinetics of **TTF**, **CN-TTF**, and **PEG3-TTF** were studied using a rotating disk electrode (RDE) to determine the diffusion coefficients (D_0) and kinetic rate constant (k_0). The RDE tests were conducted using a 1 mM **TTF** solution under an argon atmosphere (Figure S12–S15). The diffusion coefficients of the redoxmers were obtained from the Koutecký–Lévich curves with varied rotating angles (Equation S1).[5,60] The diffusion coefficients of all **TTF** compounds were of the order of 10^{-5} or 10^{-6} $cm^2\ s^{-1}$ (Table S4), suggesting that the attached chains had a negligible negative effect on the electrochemical kinetics. These values are also consistent with those of the reported redox active materials (5.39×10^{-6} $cm^2\ s^{-1}$ for TEMPO and 6.80×10^{-6} $cm^2\ s^{-1}$ for ferrocene) and are suitable for flow batteries.[61-65] The kinetic rate constants (k_0) of all **TTF** molecules, acquired by fitting the Butler–Volmer equation (Equation S2), were in the range of 10^{-4}–10^{-2} cm s^{-1} (Figures S12–S15 and Table S4), which are comparable with those of several reported redox systems,[66,67] though the attachment of the PEG chains does slow the kinetics when compared to some non-PEG derivatized organic compounds. [68,69]

Battery Performance. Considering the solubility performances of the different **TTFs**, we adopted different battery configuration strategies to maximize their potential. Insoluble **TTF** and **CN-TTF** were studied in aqueous slurry batteries using Zn as the pairing anode, while **PEG3-TTF** with high solubility was investigated in solution-based nonaqueous flow batteries using Li metal as the anode, as presented in detail below.[70]

Slurry battery using TTF and CN-TTF

Slurry screening. To achieve high-performance aqueous slurry-flow batteries, a uniform suspension of redox and additive conductive materials is required. Owing to their low molecular polarity and high

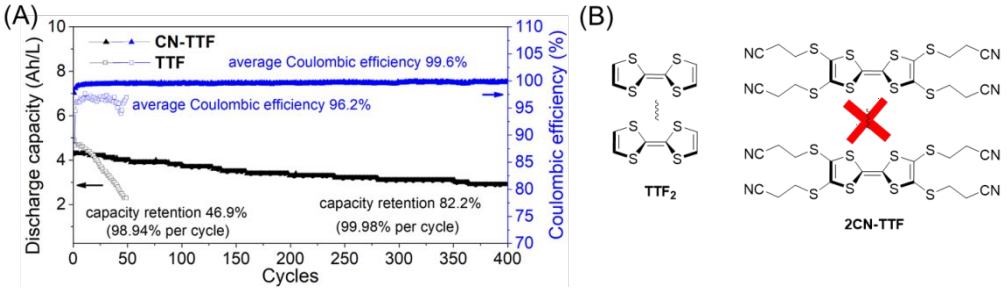

Figure 2. (A) Long-term cyclability and the Coulombic efficiency of 0.5 M Zn/**TTF** and 0.5 M Zn/**CN-TTF** batteries. (B) Demonstration of the dimerization of **TTF** and **CN-TTF.**

molecular coplanarity, **TTF** molecules tend to aggregate in water and do not disperse uniformly as a slurry.[49,71] The introduction of side chains significantly reduces the molecular coplanarity and improves the dispersity of **CN-TTF** in an aqueous electrolyte. The slurry was, prepared by grinding **TTF** or **CN-TTF** with the conductive additive Ketjen Black (KB), which is well known to form a conductive carbon-percolation network in non-conducting organic redox slurry systems and has been successfully used in slurry battery systems.[43,44,72] To study the effects of KB loading on the conductivity of the slurry electrochemical impedance spectroscopy (EIS) analysis was performed using a three-electrode setup (Figure S16). Slurries with different KB**/CN-TTF** ratios were dropped onto the surface of carbon paper to prepare the working electrode. The charge-transfer resistance (R_{ct}) in the mid-frequency region (~10^6 Hz) is the main focus of the present evaluation because it reflects the resistance to transfer charge from the current collector to the electrode surface, which, in the present case, represents the entire charge transfer in the slurry electrode.[73,74] At low KB loadings (10 and 20 g/L), high R_{ct} values (1535 Ω for 10 g/L and 1120 Ω for 20 g/L) were obtained, presumably because a limited amount of KB could not form a conductive network with the nonconductive **CN-TTF**. The R_{ct} value decreased drastically to 31.12, 8.646, and 12.30 Ω for KB loadings of 30, 40, and 50 g/L, respectively, indicating the formation of a conductive network between the interconnecting KB and **CN-TTF** molecules. Interestingly, at higher KB loadings of 60, 70, and 80 g/L, R_{ct} values increased dramatically to 10,000, 11,500, and 42,680 Ω, respectively, presumably because of the formation of KB aggregates (Figure S16). After screening the KB loading, high-resolution scanning electron microscopy (SEM) and energy dispersive X-ray spectroscopy (EDS) (Figure S17 and S18) were conducted to obtain information about the microstructure and elemental distribution of the 40 g/L **TTF/**KB and **CN-TTF/**KB slurries, suggesting that both **TTF** and **CN-TTF** were evenly distributed without aggregation.

TTF and CN-TTF slurry battery tests. Zn is used as the anolyte in slurry battery studies because of its promising redox potential and excellent water compatibility.[75,76] Zn/slurry batteries were assembled to evaluate their long-term cycling stability (Figure S19). To mitigate the hydrophobicity-induced aggregation of **TTF**, 5% tetraethylene glycol dimethyl ether (TEGDME) was used as an auxiliary dispersant. In this case, the 0.5 M Zn/**TTF** slurry battery was galvanostatically charged/discharged at 1 mA/cm^2 in the voltage range of 0.8–1.7 V. Surprisingly, three charging platforms were found in the charge/discharge profile (Figure S20A), suggesting that the mechanism of the **TTF** redox reaction in the battery is different from the normal two one-electron redox processes in solution (Figure S21). The unusual redox behavior of **TTF** in the solid state is presumably due to **TTF** dimerization (Figure S22).[54,77]

The same redox behavior (three oxidation peaks and three reduction peaks) was observed in the solid CV test, in which the KB/**TTF** slurry was deposited on a carbon paper-working electrode (Figure S23). However, the additional redox process does not introduce substantial advantages to the battery system because it does not increase the theoretical capacity or potential. After 50 cycles, the Zn/**TTF** battery exhibited an average Coulombic efficiency of 96.2% and a capacity retention of 46.9%, corresponding to a decay

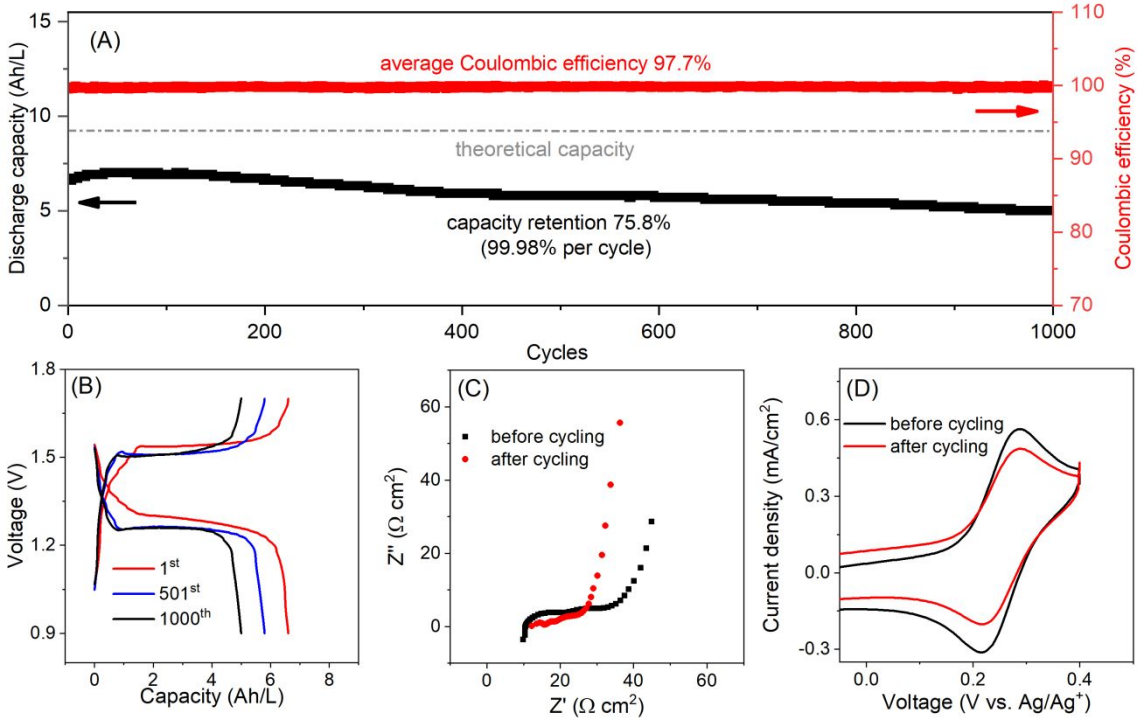

Figure 3. Long-term cyclability of the 1.0 M Zn/**CN-TTF** battery. (A) Discharge capacity and Coulombic efficiency over 1000 cycles. (B) Charge/discharge profiles for different cycles. (C) Electrochemical impedance spectra before and after cycling. (D) CV scans of the **CN-TTF** extract before and after cycling in 0.1 M $TBAPF_6$/dimethyl sulfoxide (DMSO) using glassy carbon as the working electrode.

rate of 1.06% per cycle (Figure 2A). Dimerization promotes **TTF** aggregation (Figure 2B), leading to the separation of the conductive agent and the active material; thus, increasing amounts of **TTF** were electrically insulated, forming dead redoxmers (see the photograph of the post-cycling electrode in Figure S24). The accumulated nonconductive **TTF** islands also become a significant limitation to electron transport in the slurry system; this increases the R_{ct} of the slurry system (Figure S20B), which explains the rapid decay of the battery capacity.

By contrast, under identical test conditions, the 0.5 M Zn/**CN-TTF** battery demonstrated improved cycle performance with a better capacity retention of 82.8% after 400 cycles (99.98% per cycle) and an improved average Coulombic efficiency of 97.6% (Figure 2A), which is a consequence of the four side chains that enhance the steric effects and suppress dimerization. Even though only one electron was utilized owing to the electrochemical limitation of water, a theoretical capacity utilization rate of 82% was achieved, in relation to 43% for the **TTF** battery (Figure S20 and 25A). The EIS changes before and after cycling are shown in Figure S11B. Compared with the negligible change in bulk resistance (R_b), the post-cycling R_{ct} value nearly doubled (from 19.2 Ω to 38.1 Ω), corresponding to the polarization increase in the charge/discharge profile (Figure S25A). To further elucidate the capacity decay mechanism, the pre- and post-cycling **CN-TTF** slurries were extracted using PC, and the extracts were subjected to ^{1}H nuclear magnetic resonance (NMR) and CV analyses. Only **CN-TTF** signals were observed (Figure S26 and S25C), suggesting that no by-products were generated.

The concentration of **CN-TTF** was further increased to 1.0 M, and the long-term cyclability of the battery was evaluated under the same conditions as those used for the 0.5 M battery. The 1.0 M Zn/**CN-TTF** battery exhibited excellent cycle performance for more than 1000 charge/discharge cycles (226 h, 9.4 d) with a capacity retention of 75.8% (99.98% per cycle). For the 1.0 M battery, the charge/discharge polarization did not increase significantly after 501 and 1000 cycles, which was also reflected by the smaller R_{ct} change observed in the EIS curve (Figure 3). The post-cycling slurry was extracted using PC and analyzed by ^{1}H NMR and CV (Figure 3D and S27). The current density of the post-electrolyte was slightly lower, suggesting a mild decrease in the amount of active **CN-TTF**, which presumably originated from self-aggregation. Attempts were made to achieve a higher energy density using a 1.5 M **CN-TTF** slurry battery (Figure S28 and S29). This battery exhibited a capacity utilization rate of 63% and a capacity retention of 90.3% after 100 cycles (99.90% per cycle), which are inferior to those of the 0.5 and 1.0 M batteries. In addition, compared with the relatively small resistance changes in the 0.5 or 1.0 M batteries, a significant resistance change (31.1 Ω) was observed for the 1.5 M battery (Figure S28). Also observed was the increased polarization as shown on the charging and discharging curve (Figure S28B). The large polarization and battery resistance may have been caused by the low fluidity of the concentrated slurry.

To verify the rate capability of the slurry battery, the 1.0 M Zn/**CN-TTF** battery was subjected to galvanostatic charge/discharge tests at current densities of 1–5 mA/cm^2 in the potential range of 0.9–1.7 V. The measured discharge capacity of the battery was 4.93 Ah/L at 1 mA/cm^2 (Figure S30), which is equivalent to 70% of the theoretical capacity (7.04 Ah/L). As the current density increased, the discharge capacity decreased owing to the increased overpotential (Figure S30B) and reached 3.03 Ah/L (43% of the theoretical capacity) at 5 mA/cm^2 (Figure S30A and B). The 1.0 M battery demonstrated desirable performance in terms of the Coulombic efficiency (CE), energy efficiency (EE), and voltage efficiency (VE) (Figure 3A). At a low current density of 1 mA/cm^2, the CE, EE, and VE were 97.8, 84.2, and 86.8%, respectively, and 98.2, 71.2, and 73.3% at 5 mA/cm^2, respectively. The **CN-TTF** slurry battery afforded an open-circuit voltage (OCV) of 0.95 V at zero state-of-charge (SOC). When the SOC increased from 10% to 90%, the corresponding OCV exhibited a stable linear increase, indicating a stable charging platform at 1.16 V (Figure S30C). The high-frequency area-specific resistance (ASR), which is derived from membranes,[30,64] contributed to ~74.4% of the overall resistance of the battery (Figure S30 C and D), suggesting that the resistance from the **CN-TTF** slurry is not significant.

Solution-based battery using PEG3-TTF. Solution-based RFBs using **PEG3-TTF** as the catholyte were studied using two different types of anolytes: viologen and Li. Viologen and its derivatives possess the advantage of two-electron activity,[18,64] whereas Li is well known as an anolyte owing to its remarkable negative potential.[78,79] The multi-electron activity and wide potential window features are conducive to improving the overall energy density.[15,28,80]

Using Viologen as the Anolyte. The viologen compound of interest (**V-TFSI**) in this study possesses two methyl units and two bis(trifluoromethane)sulfonimide (TFSI) anions to impart desired solubility in organic electrolytes and displays two redox couples at –0.71 V and –1.12 V vs. Ag/Ag$^+$ (Figure S31). Thus, the **V- TFSI**/**PEG3-TTF** pair provides cell voltages of 0.93 V and 1.59 V for single- and double-electron utilization (Figure S32). The single-electron 120 mM **V-TFSI** and 100 mM **PEG3-TTF** symmetric flow batteries exhibited an excellent capacity retention of 97.7% after 100 cycles (99.98% per cycle) with an average CE of 94% (Figure S33A). The nearly identical charging/discharging profiles at different cycles and slight impedance change indicate that battery polarization does not increase significantly during cycling, validating the high cyclability (Figure S33B and C). The CV results of both the catholyte and anolyte before and after battery cycling (Figure S33D) suggest that no electrochemically active by-products were generated. Subsequently, a **V-TFSI**/**PEG3-TTF** symmetric flow battery was assembled for double-electron utilization. Unfortunately, the battery could not operate normally owing to severe volume changes of the positive and negative electrolytes, presumably induced by the difference in osmotic pressure in the electrolyte.[81] Excessive consumption of active materials, pronounced crossover, and low Coulombic efficiency prompted us to discontinue the study employing a symmetric viologen system.

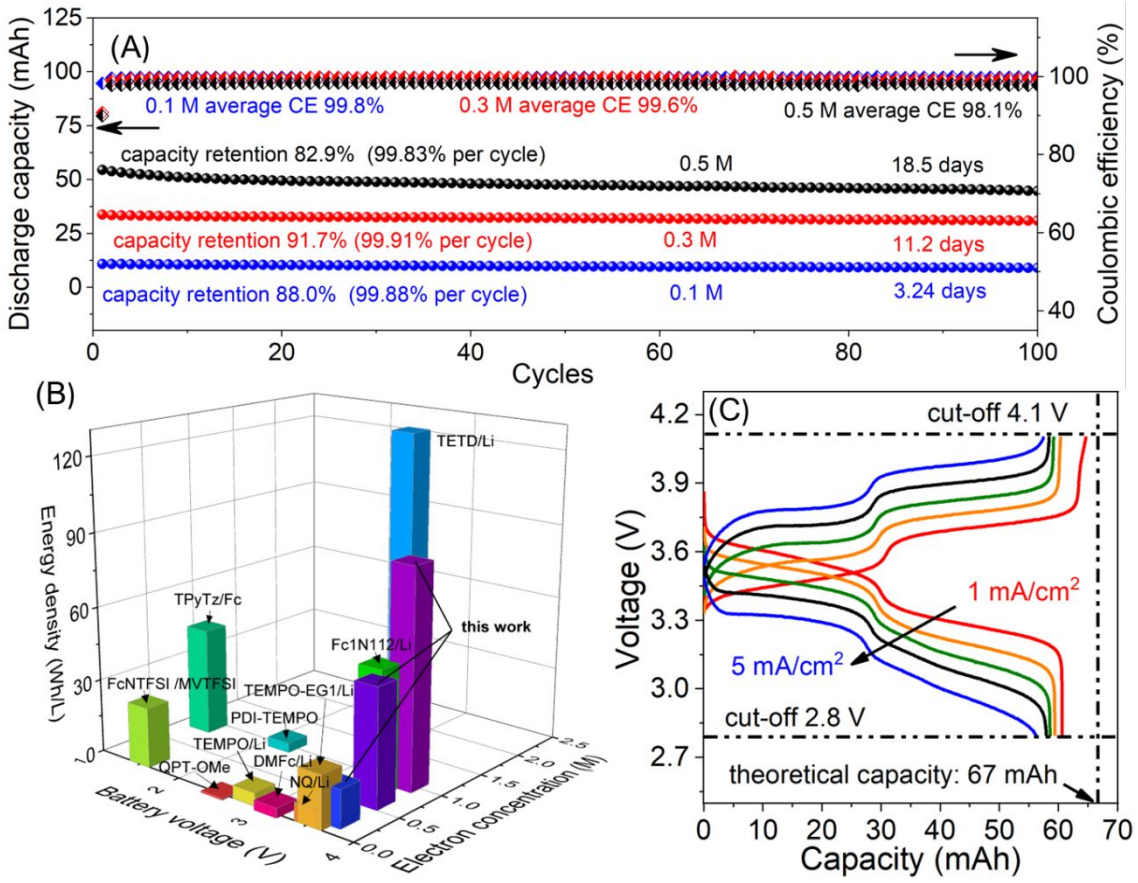

Figure 4. (A) Discharge capacity and Coulombic efficiency (CE) of 0.1 M, 0.3 M, and 0.5 M Li/**PEG3-TTF** batteries over 100 cycles. (B) Comparison of energy densities, corresponding battery voltages, and electron concentrations of **PEG3-TTF** and redoxmers in previous nonaqueous flow batteries. **DMFc** (1,1-dimethylferrocene),[82] **TEMPO** (2,2,6,6-tetramethylpiperidine-1-oxyl),[83] **TEMPO-EG1** (ethylene glycol grafted 2,2,6,6-tetramethylpiperidine-1-oxyl),[84] **NQ** (1,4-naphthoquinone),[85] **Fc1N112-TFSI**, **FcNTFSI** (ferrocenyl`methyl dimethyl ethyl ammonium bis(trifluoromethanesulfonyl)imide)[32], **TPyTz** (2,4,6-tris[1-(trimethylamonium)propyl-4-pyridiniumyl]-1,3,5-triazine hexachloride),[86] **PDI-TEMPO** (pyromellitic diimide-2,2,6,6-tetramethylpiperidine 1-oxyl),[87] **QPT-OMe** (11-methoxy-9*H*-quinolino[3,2,1-*kl*]phenothiazin-9-one),[88] and tetraethylthiuram disulfide (**TETD**)[63]. (C) Rate performance of the 0.5 M **PEG3-TTF** battery: charge/discharge profiles at different current densities.

Using Li as the Anolyte. To overcome the osmotic pressure problem and improve the energy density, asymmetric batteries with different **PEG3-TTF** concentrations (0.1 M, 0.3 M, and 0.5 M) employing Li metal as the anode, 1 M $LiPF_6$ EC/EMC (v 1:1 with 2% fluoroethylene carbonate (FEC) and 1% vinylene carbonate (VC) solution) as the electrolyte, and an anion exchange membrane (Fumasep® FAB-PK-130) were studied to explore the feasibility of two-electron utilization of **PEG3-TTF**. All the Li/**PEG3-TTF** RFBs were subjected to galvanostatic charge/discharge tests at 3 mA/cm^2 wherein the cut-off voltages were set at 2.8–4.1 V. The 0.1 M Li/**PEG3-TTF** RFBs presented capacity retentions of 99.88% per cycle and 88.0% for all the 100 cycles with an average CE of 99.8%, excluding the first cycle affected by SEI formation (Figure 4A). The charge/discharge profiles are also presented in Figure S34, showing two stable redox platforms at 3.44 V and 3.64 V and a capacity utilization of 10.8 mAh over the theoretical capacity of 13.4 mAh. The 0.3 M Li/**PEG3-TTF** battery exhibited a capacity retention of 99.91% per cycle and 91.7% after 100 cycles, and exhibited a discharge capacity of 13.5 Ah/L with an average CE of 99.6%. The charge/discharge curves at different cycles showed stable double-electron redox processes (Figure S35). For a higher energy density, the concentration of **PEG3-TTF** was further increased to 0.5 M (viscosity 24 cp), corresponding to a 1.0 M electron concentration. This battery demonstrated a capacity retention of 99.83% per cycle and 82.9% after 100 cycles over 18 d (Figure 4A and S36). In addition, a second long-term cycling test of the 0.5 M Li/**PEG3-TTF** battery was conducted to verify the repeatability (Figure S37). Benefiting from the high concentration and cell voltage, the energy density of the 0.5 M battery also attains 88.18 Wh/L, which is comparable to those of the state-of-the-art nonaqueous RFBs (Tables S5–6, Figure 4B, and Equation S4).

Even though the capacity decay was not prominent, several measurements were conducted to analyze the possible capacity-fading mechanism. (1) The high affinity of **PEG3-TTF** for the membrane. EDS element-mapping tests were conducted to obtain

information on sulfur distribution in the membrane before and after cycling (Figure S38). Sulfur is of interest as a characteristic element because it exists only in **PEG3-TTF** in the entire battery system. Sulfur was detected on the membrane after cycling (Figure S38B and S38D), suggesting that trace amounts of **PEG3-TTF** were irreversibly trapped in the membrane; [31,72] (2) impedance increased on the Li anode. During the cyclability studies of RFBs at different concentrations, we observed a distinct increase in impedance and increased polarization (Figure S34B, S35B and S36B), which may be attributed to the formation of a thick SEI layer on the surface of the Li anode, which is a common phenomenon in Li batteries.[89,90] To test the hypothesis, we replaced the anode side with fresh Li metal, electrolyte, and carbon felt after 40 cycles (Figure S39A), leading to remarkable polarization reduction (Figure S39B) and a discharge capacity increase from 51.3 mAh to 53.9 mAh, indicating that increased polarization in the anolyte is a non-negligible contributing factor in battery capacity decay; and (3) crossover. While distinct crossover was not observed in the 0.1 M- and 0.3 M-**PEG3-TTF** batteries (Figure S34D and S35D), ~2.4 mM **PEG3-TTF**, as determined by the CV current intensity, was observed in the post-cycling anolyte in the 0.5 M battery after a long-term cycling of more than 18 d (Figure S36D). The low concentration of crossed **PEG3-TTF** (<0.5 mol%) suggests that crossover may not be a major contributing factor.

The rate performance of the battery was studied by galvanostatic charge/discharge measurements at varying current densities (Figure 4C). As the current density increases from 1 to 5 mA/cm^2, the 0.5 M Li/**PEG3-TTF** battery delivered a discharge capacity of 60.6 mAh (90.4% of the theoretical capacity), 59.4 mAh (88.6% of the theoretical capacity), 58.6 mAh (87.4% of the theoretical capacity), 57.9 mAh (86.4% of the theoretical capacity), and 56.1 mAh (83.8% of the theoretical capacity), respectively. At a current density of 1 mA/cm^2, the battery exhibited a CE of 93.8%, an EE of 89.3%, and a VE of 95.1% (Figure. S40). At 5 mA/cm^2, those efficiencies were maintained at 97.7, 79.3, and 81.1%, respectively. The 0.5 M Li/**PEG3-TTF** also showed a nearly linear increase in OCV from 3.39 V at 25% SOC to 3.73 V at 100% SOC (Figure S41A). The high-frequency ASR, which predominantly reflects the resistance of the separator, contributes ~72.5% of the polarization ASR of the battery (Figure S41B and S41C). In addition, the highest current power density of ~68 mW/cm^2 was observed at 100% SOC. This power density is comparable with some reported nonaqueous RFBs.[91,92]

It has come to our attention that **TTF** has been utilized as an active material in the realm of flow batteries. Over the course of the previous year, researchers such as Chen,[93] Fujimoto,[94] and Janssen[95] have made successive reports on their work involving the implementation of TTF in flow batteries. We have included a summarized table (Table S7) including critical battery performance parameters from this work and that of other works. Our batteries demonstrate a minimum of a 60% enhancement in the two principal parameters of energy density and capacity retention. Therefore, the nonaqueous flow battery system that we have developed showcases a significant advancement in terms of performance, as opposed to a mere incremental improvement.

Conclusions

In summary, **TTF** and its derivatives were systematically studied in terms of their molecular derivatization, physical and electrochemical properties, and battery-cycling performance. As a new type of catholyte for flow battery applications, these compounds exhibited high chemical and electrochemical stability in aqueous and nonaqueous electrolytes. The introduction of four cyanoethyl chains drastically mitigated the incompatibility of the highly hydrophobic **TTF** group with the aqueous electrolyte. Moreover, the side chains introduce steric hindrance between the **TTF** frameworks to successfully suppress the detrimental dimerization and thus alleviate the capacity decay. Paired with a Zn anolyte, the 1.0 M **CN-TTF** slurry battery exhibited a capacity retention of 75.8% (99.98% per cycle) after 1000 cycles (~9.4 d) with an average Coulombic efficiency of 99.7%. However, the functionalization of **TTF** with four PEG chains drastically changed its physical state from solid to liquid, thus allowing full miscibility with organic solvents. The resulting compound, **PEG3-TTF**, presents an opportunity to develop a high-solubility electrolyte (1.0 M electron concentration) in an organic electrolyte with a high battery voltage (up to 3.64 V) and a high energy density of over 88 Wh/L. This study not only introduces a new family of compounds for flow battery applications but also demonstrates the viability of the molecular engineering strategy for enabling the application of organic redox materials in both slurry- and solution-based batteries. Moving forward, we plan to study Zn/**CN-TTF** slurry batteries under flow conditions, even though difficulties, such as high viscosity, flow resistance, and pump losses, are anticipated. Injecting or piston-driven pumps have shown promise as reliable solutions for handling high-viscosity slurries. [96-98] For non-aqueous Li/**PEG3-TTF** flow cells, the paramount task is to develop ion-exchange membranes with high ion conductivity that are compatible with non-aqueous solvents. This is of utmost importance for enhancing current density and power density in non-aqueous flow batteries.

Author Contributions

X.W., J.C., and J.J. conceived and designed the experiments. X.W., and R.S. carried out the battery experiments. X.W., R.K.G and R.S. analyzed the data. X.W. drafted the manuscript. A.L., J.J.M, and G.N. synthesized the compounds. P.S. performed NMR measurements and analysis. J.J. analyzed the data and edited the manuscript. All authors discussed the results and commented on the manuscript.

Conflicts of interest

The authors declare no conflict of interest.

Acknowledgements

This study was supported by the National Science Foundation un-der grant no. CBET-2112798. NMR experiments were

performed on a Bruker AVANCE NEO 400 MHz NMR spectrometer that was funded by the NSF-MRI grant CHE-1726092. We thank Prof. Konstantinos D. Vogiatzis from the University of Tennessee for helpful discussions from a computation perspective.

References

1. G. Resch, A. Held, T. Faber, C. Panzer, F. Toro and R. Haas, *Energy Policy*, 2008, **36**, 4048–4056.
2. T. M. Gür, *Energy Environ. Sci.*, 2018, **11**, 2696–2767.
3. S. Bai, X. Liu, K. Zhu, S. Wu and H. Zhou, *Nat. Energy*, 2016, **1**, 16094.
4. K. Xu, *Chem. Rev.*, 2004, **104**, 4303–4417.
5. B. Huskinson, M. P. Marshak, C. Suh, S. Er, M. R. Gerhardt, C. J. Galvin, X. Chen, A. Aspuru-Guzik, R. G. Gordon and M. J. Aziz, *Nature*, 2014, **505**, 195–198.
6. T. Janoschka, N. Martin, U. Martin, C. Friebe, S. Morgenstern, H. Hiller, M. D. Hager and U. S. Schubert, *Nature*, 2015, **527**, 78–81.
7. J. Noack, N. Roznyatovskaya, T. Herr and P. Fischer, *Angew. Chem. Int. Ed.*, 2015, **54**, 9776–9809.
8. B. R. Schrage, B. Zhang, S. C. Petrochko, Z. Zhao, A. Frkonja-Kuczin, A. Boika and C. J. Ziegler, *Inorg. Chem.*, 2021, **60**, 10764–10771.
9. Z. Zhao, B. Zhang, B. R. Schrage, C. J. Ziegler and A. Boika, *ACS Appl. Energy Mater.*, 2020, **3**, 10270–10277.
10. H. Huang, R. Howland, E. Agar, M. Nourani, J. A. Golen and P. J. Cappillino, *J. Mater. Chem. A*, 2017, **5**, 11586–11591.
11. J. Egitto, T. C. Gokoglan, S. K. Pahari, J. N. Bolibok, S. R. Aravamuthan, F. Liu, X. Jin, P. J. Cappillino and E. Agar, *J. Electrochem. Energy Convers. Storage*, 2022, **19**, 041005.
12. M. Vins and M. Sirovy, *2020 International Conference on Applied Electronics (AE)*, 2020, 1–5.
13. Y. Zhang, T.-T. Zuo, J. Popovic, K. Lim, Y.-X. Yin, J. Maier and Y.-G. Guo, *Mater. Today*, 2020, **33**, 56–74.
14. F. Wu, J. Maier and Y. Yu, *Chem. Soc. Rev.*, 2020, **49**, 1569–1614.
15. X. Wei, W. Pan, W. Duan, A. Hollas, Z. Yang, B. Li, Z. Nie, J. Liu, D. Reed, W. Wang and V. Sprenkle, *ACS Energy Lett.*, 2017, **2**, 2187–2204.
16. Y. Jing, E. M. Fell, M. Wu, S. Jin, Y. Ji, D. A. Pollack, Z. Tang, D. Ding, M. Bahari, M.-A. Goulet, T. Tsukamoto, R. G. Gordon and M. J. Aziz, *ACS Energy Lett.*, 2021, **7**, 226–235.
17. C. Zhang, Z. Niu, S. Peng, Y. Ding, L. Zhang, X. Guo, Y. Zhao and G. Yu, *Adv. Mater.*, 2019, **31**, e1901052.
18. M. Pan, Y. Lu, S. Lu, B. Yu, J. Wei, Y. Liu and Z. Jin, *ACS Appl. Mater. Interfaces*, 2021, **13**, 44174–44183.
19. J. Luo, B. Hu, M. Hu, W. Wu and T. L. Liu, *Angew. Chem. Int. Ed.*, 2022, **64**, e202204030.
20. Z. Chang, D. Henkensmeier and R. Chen, *J. Power Sources*, 2019, **418**, 11–16.
21. K. Lin, Q. Chen, M. R. Gerhardt, L. Tong, S. B. Kim, L. Eisenach, A. W. Valle, D. Hardee, R. G. Gordon and M. J. Aziz, *Science*, 2015, **349**, 1529–1532.
22. M. R. Tuttle and S. Zhang, *Chem. Mater.*, 2019, **32**, 255–261.
23. C. S. Sevov, D. P. Hickey, M. E. Cook, S. G. Robinson, S. Barnett, S. D. Minteer, M. S. Sigman and M. S. Sanford, *J. Am. Chem. Soc.*, 2017, **139**, 2924–2927.
24. C. S. Sevov, S. L. Fisher, L. T. Thompson and M. S. Sanford, *J. Am. Chem. Soc.*, 2016, **138**, 15378–15384.
25. B. Hu, C. DeBruler, Z. Rhodes and T. L. Liu, *J. Am. Chem. Soc.*, 2017, **139**, 1207–1214.
26. M. A. Goulet, L. Tong, D. A. Pollack, D. P. Tabor, E. E. Kwan, A. Aspuru-Guzik, R. G. Gordon and M. J. Aziz, *J. Am. Chem. Soc.*, 2019, **141**, 8014–8019.
27. Y. Yan, R. Walser-Kuntz and M. S. Sanford, *ACS Mater. Lett.*, 2022, DOI: 10.1021/acsmaterialslett.2c00050, 733–739.
28. X. Fang, Z. Li, Y. Zhao, D. Yue, L. Zhang and X. Wei, *ACS Mater. Lett.*, 2022, 277–306.
29. B. H. Hu, J. L. Luo, M. Hu, B. Y. Yuan and T. L. Liu, *Angew. Chem. Int. Ed.*, 2019, **58**, 16629–16636.
30. S. Jin, Y. Jing, D. G. Kwabi, Y. Ji, L. Tong, D. De Porcellinis, M.-A. Goulet, D. A. Pollack, R. G. Gordon and M. J. Aziz, *ACS Energy Lett.*, 2019, **4**, 1342–1348.
31. J. Chai, X. Wang, A. Lashgari, C. K. Williams and J. Jiang, *ChemSusChem*, 2020, **13**, 4069–4077.
32. B. Hu and T. L. Liu, *J. Energy Chem.*, 2018, **27**, 1326–1332.
33. T. Janoschka, N. Martin, M. D. Hager and U. S. Schubert, *Angew. Chem. Int. Ed.*, 2016, **55**, 14427–14430.
34. X. Wei, L. Cosimbescu, W. Xu, J. Z. Hu, M. Vijayakumar, J. Feng, M. Y. Hu, X. Deng, J. Xiao, J. Liu, V. Sprenkle and W. Wang, *Adv. Energy Mater.*, 2015, **5**, 1400678.
35. R. Yan and Q. Wang, *Adv. Mater.*, 2018, **30**, e1802406.
36. W. Yan, C. Wang, J. Tian, G. Zhu, L. Ma, Y. Wang, R. Chen, Y. Hu, L. Wang, T. Chen, J. Ma and Z. Jin, *Nat. Commun.*, 2019, **10**, 2513.
37. Q. Huang, H. Li, M. Gratzel and Q. Wang, *Phys. Chem. Chem. Phys.*, 2013, **15**, 1793–1797.
38. C. Jia, F. Pan, Y. G. Zhu, Q. Huang, L. Lu and Q. Wang, *Sci. Adv.*, 2015, **1**, e1500886.
39. J. R. Jennings, Q. Huang and Q. Wang, *J. Phys. Chem. C*, 2015, **119**, 17522–17528.
40. J. Ye, L. Xia, C. Wu, M. Ding, C. Jia and Q. Wang, *J. Phys., D, Appl. Phys.*, 2019, **52**, 443001.
41. S. H. Oh, C. W. Lee, D. H. Chun, J. D. Jeon, J. Shim, K. H. Shin and J. H. Yang, *J. Mater. Chem. A*, 2014, **2**, 19994–19998.
42. T. J. Petek, N. C. Hoyt, R. F. Savinell and J. S. Wainright, *J. Power Sources*, 2015, **294**, 620–626.
43. X. Xing, Q. Liu, J. Li, Z. Han, B. Wang and J. P. Lemmon, *Chem. Commun.*, 2019, **55**, 14214–14217.
44. X. Zhang, W. Li and H. Chen, *ACS Appl. Mater. Interfaces*, 2021, **13**, 40552–40561.
45. F. Wudl, G. Smith and E. Hufnagel, *J. Chem. Soc., Chem. Commun.*, 1970, **21**, 1453–1454.
46. J. Ferraris, D. Cowan, V. t. Walatka and J. Perlstein, *J. Am. Chem. Soc.*, 1973, **95**, 948–949.
47. D. Canevet, M. Salle, G. Zhang, D. Zhang and D. Zhu, *Chem. Commun.*, 2009, **17**, 2245–2269.
48. N. Duvva, U. Chilakamarthi and L. Giribabu, *Sustain. Energy Fuels*, 2017, **1**, 678–688.
49. A. Jana, M. Ishida, J. S. Park, S. Bahring, J. O. Jeppesen and J. L. Sessler, *Chem. Rev.*, 2017, **117**, 2641–2710.
50. Y. G. Weng, W. Y. Yin, M. Jiang, J. L. Hou, J. Shao, Q. Y. Zhu and J. Dai, *ACS Appl. Mater. Interfaces*, 2020, **12**, 52615–52623.
51. Y. Misaki, S. Noda, M. Kato, T. Yamauchi, T. Oshima, A. Yoshimura, T. Shirahata and M. Yao, *ChemSusChem*, 2020, **13**, 2312–2320.
52. M. Kato, K.-i. Senoo, M. Yao and Y. Misaki, *J. Mater. Chem. A*, 2014, **2**, 6747–6754.
53. Y. Ding, C. Zhang, L. Zhang, Y. Zhou and G. Yu, *Chem. Soc. Rev.*, 2018, **47**, 69–103.
54. M. Hasegawa and M. Iyoda, *Organic Redox Systems: Synthesis, Properties, and Applications,(Ed.: T. Nishinaga), Wiley*, 2015, 89–125.

55. J. Y. Becker, J. Bernstein, A. Ellern, H. Gershtenman and V. Khodorkovsky, *J. Mater. Chem.*, 1995, **5**, 1557–1558.
56. H. V. Schroder and C. A. Schalley, *Beilstein J. Org. Chem.*, 2018, **14**, 2163–2185.
57. J. Zhang, J. Huang, L. A. Robertson, R. S. Assary, I. A. Shkrob and L. Zhang, *J. Phys. Chem. C*, 2018, **122**, 8116–8127.
58. K. H. Hendriks, C. S. Sevov, M. E. Cook and M. S. Sanford, *ACS Energy Lett.*, 2017, **2**, 2430–2435.
59. X. Wang, J. Chai, A. Lashgari and J. J. Jiang, *ChemElectroChem*, 2020, **8**, 83–89.
60. C. DeBruler, B. Hu, J. Moss, X. Liu, J. Luo, Y. Sun and T. L. Liu, *Chem*, 2017, **3**, 961–978.
61. J. Zhang, Z. Yang, I. A. Shkrob, R. S. Assary, S. o. Tung, B. Silcox, W. Duan, J. Zhang, C. C. Su, B. Hu, B. Pan, C. Liao, Z. Zhang, W. Wang, L. A. Curtiss, L. T. Thompson, X. Wei and L. Zhang, *Adv. Energy Mater.*, 2017, **7**, 1701272.
62. J. Luo, W. Wu, M. Hu, B. Yuan and T. Liu, *Energy Environ. Sci.*, 2022, **15**, 1315–1324.
63. L. Zhang, B. Zhao, C. Zhang and G. Yu, *Angew. Chem. Int. Ed.*, 2021, **60**, 4322–4328.
64. J. Chai, A. Lashgari, Z. Cao, C. K. Williams, X. Wang, J. Dong and J. Jiang, *ACS Appl. Mater. Interfaces*, 2020, **12**, 15262–15270.
65. G. S. Nambafu, K. Siddharth, C. Zhang, T. Zhao, Q. Chen, K. Amine and M. Shao, *Nano Energy*, 2021, **89**, 106422.
66. Y. Qin, K. Holguin, D. Fehlau, C. Luo and T. Gao, *ACS Appl. Energy Mater.*, 2022, **5**, 2675–2678.
67. S. R. Bheemireddy, Z. Li, J. Zhang, G. Agarwal, L. A. Robertson, I. A. Shkrob, R. S. Assary, Z. Zhang, X. Wei, L. Cheng and L. Zhang, *ACS Appl. Mater. Interfaces*, 2022, **14**, 28834–28841.
68. M. J. Baran, M. N. Braten, E. C. Montoto, Z. T. Gossage, L. Ma, E. Chénard, J. S. Moore, J. Rodríguez-López and B. A. Helms, *Chem. Mater.*, 2018, **30**, 3861–3866.
69. M. V. Makarova, A. V. Akkuratov, M. E. Sideltsev, K. J. Stevenson and E. I. Romadina, *ChemElectroChem*, 2022, **9**, e202200483.
70. T. Tan, Y.-M. Chiang, N. Ota, T. Wilder and M. Duduta, Asymmetric battery having a semi-solid cathode and high energy density anoder, 2022, U. S. DoE, 24M Technologies, Inc., Cambridge, MA (United States)
71. Y. Kashimura, T. Goto, H. Nakashima, K. Furukawa, E. Wang, H. Li, W. Hu and K. Torimitsu, *Jpn. J. Appl. Phys.*, 2010, **49**, 01AB08.
72. X. Wang, J. Chai, S. Zhang, B. Chen, A. Chaturvedi, G. Cui and J. J. Jiang, *ACS Energy Lett.*, 2022, **7**, 1178–1186.
73. B. L. Corso, I. Perez, T. Sheps, P. C. Sims, O. T. Gül and P. G. Collins, *Nano Lett.*, 2014, **14**, 1329–1336.
74. A. J. Bard and L. R. Faulkner, *Electrochem. Methods*, 2001, **2**, 580–632.
75. L. Ma, M. A. Schroeder, O. Borodin, T. P. Pollard, M. S. Ding, C. Wang and K. Xu, *Nat. Energy*, 2020, **5**, 743–749.
76. J. Xie, F. Yu, J. Zhao, W. Guo, H.-L. Zhang, G. Cui and Q. Zhang, *Energy Stor. Mater.*, 2020, **33**, 283–289.
77. M. Iyoda, M. Hasegawa and Y. Miyake, *Chem. Rev.*, 2004, **104**, 5085–5114.
78. P. Mu, H. Zhang, H. Jiang, T. Dong, S. Zhang, C. Wang, J. Li, Y. Ma, S. Dong and G. Cui, *J. Am. Chem. Soc.*, 2021, **143**, 18041–18051.
79. G. Xu, J. Li, C. Wang, X. Du, D. Lu, B. Xie, X. Wang, C. Lu, H. Liu and S. Dong, *Angew. Chem. Int. Ed.*, 2021, **133**, 7849–7855.
80. J. Luo, B. Hu, M. Hu, Y. Zhao and T. L. Liu, *ACS Energy Lett.*, 2019, **4**, 2220–2240.
81. P. Fischer, P. Mazur and J. Krakowiak, *Molecules*, 2022, **27**, 560.
82. G. Cong, Y. Zhou, Z. Li and Y.-C. Lu, *ACS Energy Lett.*, 2017, **2**, 869–875.
83. X. Wei, W. Xu, M. Vijayakumar, L. Cosimbescu, T. Liu, V. Sprenkle and W. Wang, *Adv. Mater.*, 2014, **26**, 7649–7653.
84. Y. Zhao, J. Zhang, G. Agarwal, Z. Yu, R. E. Corman, Y. Wang, L. A. Robertson, Z. Shi, H. A. Doan, R. H. Ewoldt, I. A. Shkrob, R. S. Assary, L. Cheng, V. Srinivasan, S. J. Babinec and L. Zhang, *J. Mater. Chem. A*, 2021, **9**, 16769–16775.
85. Y. Ding, Y. Li and G. Yu, *Chem*, 2016, **1**, 790–801.
86. J. Huang, S. Hu, X. Yuan, Z. Xiang, M. Huang, K. Wan, J. Piao, Z. Fu and Z. Liang, *Angew. Chem. Int. Ed.*, 2021, **60**, 20921–20925.
87. G. S. Nambafu, E. P. Delmo, U. Bin Shahid, C. Zhang, Q. Chen, T. Zhao, P. Gao, K. Amine and M. Shao, *Nano Energy*, 2022, **94**, 106963.
88. Y. Liu, G. Dai, Y. Chen, R. Wang, H. Li, X. Shi, X. Zhang, Y. Xu and Y. Zhao, *ACS Energy Lett.*, 2022, 1274–1283.
89. Y. Li, K. Leung and Y. Qi, *Acc. Chem. Res.*, 2016, **49**, 2363–2370.
90. A. Wang, S. Kadam, H. Li, S. Shi and Y. Qi, *Npj Comput. Mater.*, 2018, **4**, 1–26.
91. Y. Zhen, C. Zhang, J. Yuan and Y. Li, *J. Mater. Chem. A*, 2021, **9**, 22056–22063.
92. L. Zhang, Y. Qian, R. Feng, Y. Ding, X. Zu, C. Zhang, X. Guo, W. Wang and G. Yu, *Nat. Commun.*, 2020, **11**, 3843.
93. W. Hu, J. Xu, N. Chen, Z. Deng, Y. Lai and D. Chen, *Green Energy Environ.*, 2022, DOI: 10.1016/j.gee.2022.10.005.
94. H. Nariyama, S. Ito, Y. Okada, Y. Inatomi, K. Ichikawa, Y. Masumoto and M. Fujimoto, *Electrochim. Acta*, 2022, **409**, 139915.
95. N. Daub, K. H. Hendriks and R. A. J. Janssen, *Batter. Supercaps*, 2022, **5**, e202200386.
96. M. Duduta, B. Ho, V. C. Wood, P. Limthongkul, V. E. Brunini, W. C. Carter and Y. M. Chiang, *Adv. Energy Mater.*, 2011, **1**, 511–516.
97. V. E. Brunini, Y.-M. Chiang and W. C. Carter, *Electrochim. Acta*, 2012, **69**, 301–307.
98. M. S. Alfonso, H. Parant, J. Yuan, W. Neri, E. Laurichesse, K. Kampioti, A. Colin and P. Poulin, *iScience*, 2021, **24**, 102456.